Bioorganic & Medicinal Chemistry Letters xxx (2018) xxx–xxx

Contents lists available at ScienceDirect

Bioorganic & Medicinal Chemistry Letters

journal homepage: www.elsevier.com/locate/bmcl

Cathepsin B inhibitors: Further exploration of the nitroxoline core

Izidor Sosič [a], Ana Mitrović [a], Hrvoje Ćurić [b], Damijan Knez [a], Helena Brodnik Žugelj [b], Bogdan Štefane [b], Janko Kos [a,c], Stanislav Gobec [a,*]

[a] Faculty of Pharmacy, University of Ljubljana, Aškerčeva 7, 1000 Ljubljana, Slovenia
[b] Faculty of Chemistry and Chemical Technology, University of Ljubljana, Večna pot 113, 1000 Ljubljana, Slovenia
[c] Department of Biotechnology, Jožef Stefan Institute, Jamova 39, 1000 Ljubljana, Slovenia

ARTICLE INFO

Article history:
Received 12 December 2017
Revised 16 January 2018
Accepted 21 February 2018
Available online xxxx

Keywords:
Human cathepsin B
Nitroxoline derivatives
Structure-activity relationships
Tumor invasion

ABSTRACT

Human cathepsin B is a cysteine protease with many house-keeping functions, such as intracellular proteolysis within lysosomes. Its increased activity and expression have been strongly associated with many pathological processes, including cancers. We present here the design and synthesis of novel derivatives of nitroxoline as inhibitors of cathepsin B. These were prepared either by omitting the pyridine part, or by modifying positions 2, 7, and 8 of nitroxoline. All compounds were evaluated for their ability to inhibit endopeptidase and exopeptidase activities of cathepsin B. For the most promising inhibitors, the ability to reduce extracellular and intracellular collagen IV degradation was determined, followed by their evaluation in cell-based *in vitro* models of tumor invasion. The presented data show that we have further defined the structural requirements for cathepsin B inhibition by nitroxoline derivatives and provided additional knowledge that could lead to non-peptidic compounds with usefulness against tumor progression.

Human cathepsin B (catB, EC 3.4.22.1) is an intracellular lysosomal cysteine protease that is ubiquitously expressed in many tissues and is involved in a number of physiological processes.[1] The enzyme possesses an endopeptidase and a dipeptidyl carboxypeptidase activity,[2] a unique feature for cysteine cathepsins that is attributed to the presence of the occluding loop.[3] This is a flexible 20 amino acid insertion that in the so-called closed (i.e., exopeptidase) conformation spans from the left domain to cover the primed subsites S3′ and S2′ of the active site cleft and prevents the access of large endopeptidase substrates.[4,5] The occluding loop is held in this conformation via two salt bridges, His110-Asp22 and Arg116-Asp224. Additionally, two histidine residues (His110 and His111) are located at its tip providing positively charged anchors for the negatively charged C-terminal carboxyl group of the substrates.[4,6] Besides the well-known exopeptidase activity that has a pH optimum of around 5.0,[7] the endopeptidase function of catB greatly increases when the ionic contacts that bind the loop to the body of the enzyme are weakened.[6] It has been shown that the endopeptidase activity of catB increases with a rising pH value, reaching its maximum at neutral pH.[7]

CatB can actively participate in the majority of processes that significantly contribute to cancer progression. Particularly, it can modify the tumor microenvironment through the turnover and degradation of the extracellular matrix (ECM) either directly via proteolytic degradation of its components or indirectly via activation or amplification of other proteases in the proteolytic cascade.[8,9] This ECM breakdown is a crucial step that promotes tumor invasion, and enables angiogenesis and metastasis.[10,11] The degradation of metalloprotease inhibitors and the release of growth factors that are bound to the ECM components are two additional mechanisms through which catB contributes to angiogenesis.[12–14] CatB was also found to have a role in chemotherapy resistance, as it was shown that lysosomal leakage of catB, caused by chemotherapeutics 5-florouracil and gemcitabine, activates the Nlrp3 inflammasome and promotes tumor growth.[15] Importantly, high pharmacological relevance of catB has also been established in various tumor mouse models using catB-deficient mice[16–20] rendering catB as a validated and druggable target for the design of new anti-tumor drugs.

Abbreviations: Abz, 2-aminobenzoyl; AMC, 7-amido-4-methylcoumarin; catB, cathepsin B; DIPEA, *N,N*-diisopropylethylamine; DMSO, dimethyl sulfoxide; ECM, extracellular matrix; EDC, 1-ethyl-3-(3-dimethylaminopropyl)carbodiimide; HATU, 1-[bis(dimethylamino)methylene]-1*H*-1,2,3-triazolo[4,5-*b*]pyridinium 3-oxid hexafluorophosphate; HOBt, hydroxybenzotriazole; K_i, inhibition constant; TBTU, *O*-(benzotriazol-1-yl)-*N,N,N′,N′*-tetramethyluronium tetrafluoroborate; Z, benzyloxycarbonyl.

* Corresponding author.
E-mail address: stanislav.gobec@ffa.uni-lj.si (S. Gobec).

https://doi.org/10.1016/j.bmcl.2018.02.042
0960-894X/

Several types of exogenous inhibitors of catB have been identified and the majority of them have peptidyl backbones that contain an electrophilic functionality in the position of the scissile peptide bond. Various electrophilic warheads were explored in preclinical studies and these form either an irreversible (epoxysuccinyl, vinyl sulfone, acyloxymethyl ketone) or a reversible (ketone, nitrile) covalent bond with the catalytic cysteine in the active site.[21] Due to their low reactivities towards other cellular nucleophiles, the nitrile-containing inhibitors are receiving the most attention in the development of inhibitors of catB,[22] as well as other cysteine cathepsins.[23,24] The peptidic nature of currently available inhibitors can be a cause of low bioavailability and poor metabolic stability, which limit the use of a best part of such compounds to research only.[25] Given the fact that researchers involved in this field continue to appreciate the importance of cathepsins in disease management[26] and their involvement in cancer progression,[27] there is a substantial need for the advances towards new catB-inhibiting scaffolds that can bypass the limitations of peptidic catB inhibitors.

Our work in the field of catB inhibitors has been focused on nitroxoline and its derivatives and is summarized in Fig. 1. On the basis of these previous results, we herein report a complementary and focused set of compounds used to further explore the chemical space and the structure-activity relationships (SARs) of nitroxoline-based derivatives. Our efforts have resulted in several compounds that inhibit both catB activities in the low micromolar range, inhibit degradation of the ECM, and concurrently reduce invasiveness in cell-based *in vitro* models of tumor invasion.

The fragment-like characteristics of the 5-nitro-8-hydroxyquinoline core of nitroxoline enable numerous possibilities for structural elaboration. In our design, we pursued four different modifications to nitroxoline (Fig. 2).

First, several different 7-carboxamido substituted derivatives were prepared. Besides incorporating substituents that were used in our previous series of 7-aminomethylated derivatives,[28,30] we focused also on amidoacetonitriles. These nitrile-based substituents are very often used as mildly electrophilic warheads in inhibitors of different cathepsins.[22] Furthermore, some of the most recent and the most potent catB inhibitors known to date possess substituents of this exact nature.[23] Next, we synthesized a variety of compounds with nitrile-based substituents, i.e., either aminoacetonitriles or amidoacetonitriles at position 2 of the 8-hydroxy-5-nitroquinoline scaffold. The underlying reason for the preparation of these compounds was based on our recent molecular dynamics studies of the binding of nitroxoline and its derivatives into the active site of catB.[32] These results indicated that the quinoline ring can rotate around the axis, which is represented by the quinoline-NO_2 bond; a characteristic that is not evident from the crystal structure of the complex.[28] In addition, docking of a representative 2-amidoacetonitrile substituted 8-hydroxy-5-nitroquinoline **22** further corroborated this approach (Figs. S1 and S2 in the Supplementary data). Thus, interactions of the nitrile group of substituents at position 2 of the nitroxoline core with the catalytic cysteine are also possible. Third, a series of truncated compounds was prepared, in which the pyridine moiety was omitted. Within this group of derivatives, the same substituents as in the 7-carboxamido group were used and all were appended at position *ortho* with respect to the hydroxyl group. By preparing truncated derivatives we wanted to determine if the *ortho* substituted 4-nitrophenol represents a sufficient pharmacophore to be recognized by catB and to enable binding in its active site. Finally, we prepared a variety of compounds with diverse substituents attached directly to position 8 of the 5-nitroquinoline ring. Despite knowing the potential toxicity issues associated with NO_2-substituted aryl derivatives, this functionality was present in the synthesized molecules from all four classes. We established previously[28,30] that NO_2 group is a prerequisite for the inhibition of catB as it interacts with two histidines, His110 and His111, in the occluding loop of catB.

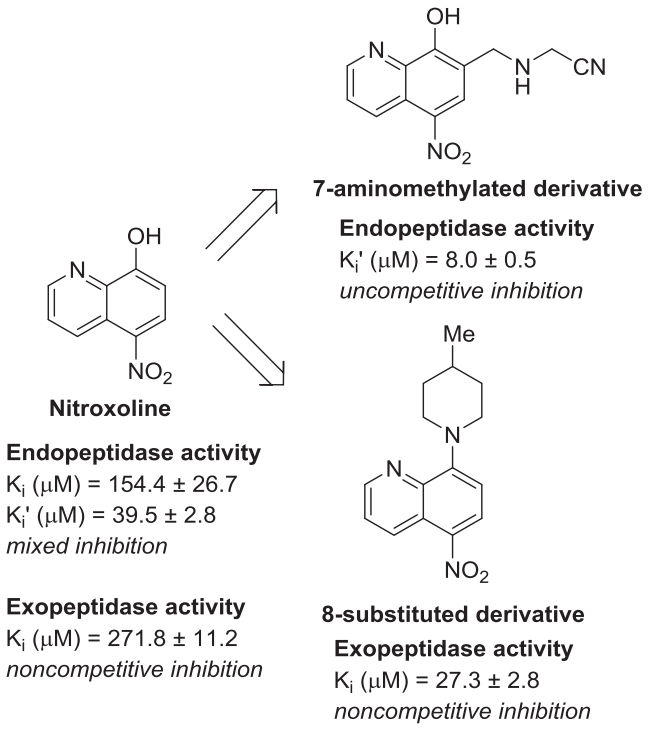

Fig. 1. Nitroxoline (5-nitro-8-hydroxyquinoline) and its endopeptidase and exopeptidase inhibition of catB.[28,29] Two representative examples of a first set of optimized derivatives[30,31] are also represented.

The nitroxoline carboxylic acid **1**[30,33] was used as substrate for the preparation of 7-carboxamido substituted nitroxoline derivatives **2**–**14** by modification of the carboxylic acid via an acid chloride (Scheme 1: rectangle A). Interestingly, all attempts to synthesize these derivatives using coupling reagents were unsuccessful. To prepare 2-substituted derivatives, five different commercially available quinolinol derivatives were used as starting material (Scheme 1: rectangle B). An efficient nitration procedure was applied in the first step using either a mixture of KNO_3/97% H_2SO_4 in acetic acid (for compounds **15** and **19**), 65% HNO_3 in acetic acid (for compounds **16** and **17**), or a mixture of 65% HNO_3/97% H_2SO_4 in acetic acid (for **18**). The regioselective introduction of the NO_2 group was confirmed by two-dimensional NMR experiments, such as homonuclear correlation spectroscopy and Nuclear Overhauser effect spectroscopy. The 2-aminoacetonitrile derivative **20** was synthesized from **18** by reductive amination procedure using $Na(OAc)_3BH$ as a reducing agent, whereas the amidoacetonitriles **21**–**24** were prepared by HATU-mediated coupling of 2-carboxy-8-hydroxy-5-nitroquinoline (**19**) and the corresponding amines (Scheme 1: rectangle B). Of note, several 2-substituted-5,7-dinitro derivatives were prepared (compounds **S1–S6**, Scheme S1 in the Supplementary data) and assayed for inhibition of catB.

For the 2-aminomethylated 4-nitrophenols **25**–**31**, either Mannich reaction conditions (**25**–**29**) or reductive amination (**30** and **31**) were used. The 2-carboxamide 4-nitrophenols **33**–**39** were synthesized via nitration of the salicylic acid to obtain intermediate **32**, followed by the reaction with $SOCl_2$ to generate the acid chloride *in situ*. Different amines were used subsequently for the formation of an amide bond in good overall yields (Scheme 1: rectangle C).

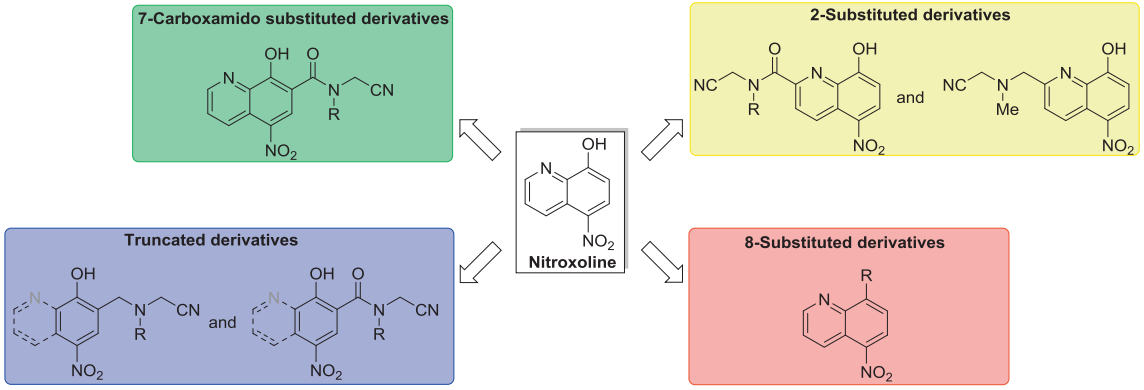

Fig. 2. Schematic representation of structural modifications to nitroxoline.

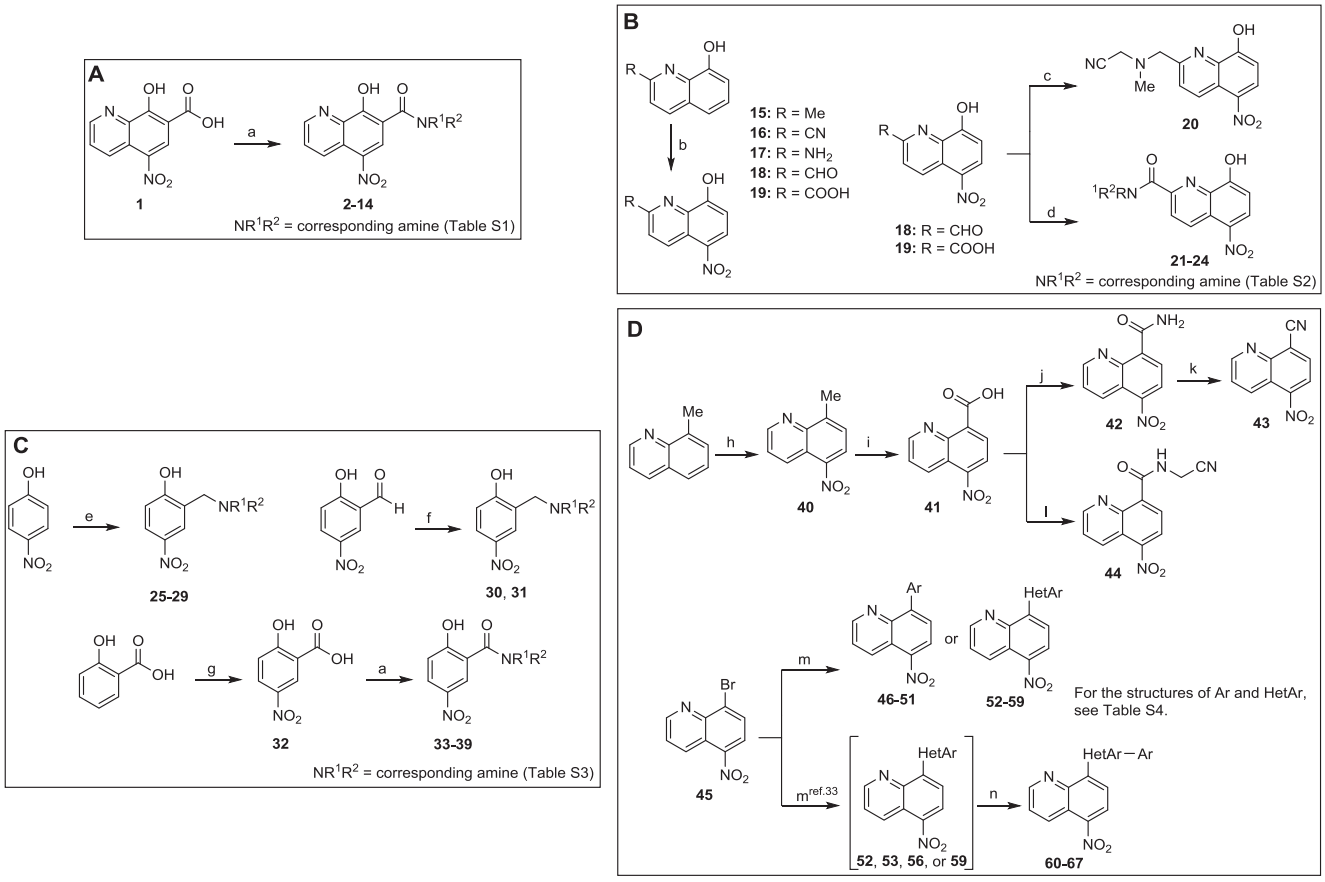

Scheme 1. Synthesis of 7-Carboxamido Substituted Derivatives (A), 2-Substituted Derivatives (B), Truncated Nitroxolines (C), and 8-Substituted Derivatives (D). [a]Reagents and conditions: (a) 1. $SOCl_2$, toluene, 80 °C, 4 h; 2. corresponding amine (R^1R^2NH, Table S1), THF, 0 °C to rt, 24 h; (b) KNO_3/97% H_2SO_4, CH_3COOH, 16 °C to rt, 1 h (for compounds **15** and **19**); 65% HNO_3, CH_3COOH, 16 °C to rt, 3 h (for **16**) or 24 h (for **17**); 65% HNO_3/97% H_2SO_4, CH_3COOH, 15–25 °C, 1 h (for **18**) (c) methylaminoacetonitrile hydrochloride, $Na(OAc)_3BH$, DIPEA, 1,2-dichloroethane, 70 °C, 24 h; (d) corresponding amine (R^1R^2NH, Table S2), HATU, DIPEA, CH_3CN, rt, 24 h; (e) corresponding amine (R^1R^2NH, Table S3), HCHO, 2-propanol, 85 °C, 24 h; (f) corresponding amine (R^1R^2NH, Table S3), $Na(OAc)_3BH$, DIPEA, 1,2-dichloroethane, rt, 24 h; (g) HNO_3, CH_3COOH, 50 °C, 15 min; (h) KNO_3/97% H_2SO_4, 0 °C to rt, 1 h; (i) 97% H_2SO_4, $K_2Cr_2O_7$, 80 °C, 1 h; (j) 1. ethyl chloroformate, Et_3N, THF, −10 °C; 2. NH_3 (g), rt, 1 h; (k) $POCl_3$/imidazole, pyridine, −30 °C, 30 min; (l) aminoacetonitrile hydrochloride, EDC, HOBt, Et_3N, DMF rt, 24 h; (m) Ar-$B(OH)_2$, $Pd(PPh_3)_4$, Cs_2CO_3, toluene, 100 °C, 24 h (for **46**–**49**) or Ar-$B(OH)_2$, Pd $(OAc)_2$, PPh_3, K_2CO_3, 1,4-dioxane/H_2O (4/1, v/v), 100 °C, 24 h (for **50** and **51**) or HetAr–$B(OH)_2$, $Pd(OAc)_2$, PPh_3, K_2CO_3, 1,4-dioxane/H_2O (4/1, v/v), 100 °C, 24 h (for **52**–**59**); (n) Ar–Br, $Pd(OAc)_2$, 120 °C, 24 h.

Diverse synthetic approaches were used to obtain 8-substituted nitroxoline analogs (Scheme 1: rectangle D). The preparation of compounds in which position 8 was substituted with a carboxylic acid derivative (compounds **41**–**44**) started from 8-methylquinoline. The most appropriate nitration reagent to successfully obtain compound **40** in a good yield (80%) was found to be an excess of KNO_3 in 97% H_2SO_4. The 8-carboxy nitroxoline derivative **41** was prepared by oxidation of the aromatic methyl group of **40** using potassium dichromate in 97% H_2SO_4. The 8-carboxamide derivative **42** was synthesized via generation of mixed anhydride by using ethyl chloroformate, followed by bubbling of the reaction mixture with ammonia. For the dehydration of the primary amide of **42** and formation 8-cyano-5-nitroquinoline (**43**), the standard $POCl_3$/imidazole mixture was utilized. Compound **44** was prepared by

EDC-mediated coupling of **41** with aminoacetonitrile hydrochloride. To prepare a series of 8-(hetero)aryl substituted quinolines **46**–**67**, an efficient methodology was developed by the Štefane group.[34] Compounds **46**–**59** were synthesized by Pd-catalyzed coupling of organoboron reagents with 8-bromo-5-nitroquinoline (**45**),[34] whereas derivatives **60**–**67** were prepared by an original one-pot sequential Suzuki-Miyaura cross-coupling/direct C—H arylation reaction (Scheme 1: rectangle D). This methodology enabled rapid access to a variety of polysubstituted molecular architectures at position 8 of the quinoline ring.

The biochemical evaluation of the synthesized compounds was initiated with the determination of their relative inhibition of catB endopeptidase and exopeptidase activities, using the catB specific substrates *Z*-Arg-Arg-7-amido-4-methylcoumarin (*Z*-Arg-Arg-AMC) and 2-aminobenzoyl (Abz)-Gly-Ile-Val-Arg-Ala-Lys(Dnp)—OH, respectively (results not shown). The compounds that showed relative inhibitions similar to nitroxoline or better at 50 μM (endopeptidase activity, 21.9% ± 3.3%; exopeptidase activity, 24.7% ± 2.8%, Fig. 1) were further characterized by determining their kinetic parameters and their mode of inhibition. In Table 1, a selection of the most potent derivatives with characterized mode of inhibition is represented; whereas the assay results for all other compounds are shown in the Supplementary data (Tables S1–S5). K_i values represent inhibition constants for the dissociation of the enzyme-inhibitor complex, whereas the K_i' values are inhibition constants for the dissociation of the enzyme-substrate-inhibitor complex.

Based on the data given in Tables 1 and in S1–S5, the structural features needed for inhibition can be deduced. In order not to overinterpret the SAR data, only the important findings are emphasized. Most of the 7-carboxamide derivatives **2**–**14** that showed catB inhibitory activity were either uncompetitive inhibitors of catB endopeptidase activity or showed mixed type of inhibition with a predominantly uncompetitive component. Very similar data was obtained when Abz-Gly-Ile-Val-Arg-Ala-Lys(Dnp)—OH was used as a substrate and the influence on the exopeptidase activity of catB was addressed, as these compounds showed the same mode of inhibition and in the same concentration range (Tables 1 and S1). In comparison with their 7-aminomethylated counterparts,[28,30] compounds **2**–**4** showed very similar inhibitory properties, whereas compounds **5**–**8** showed 2–10-fold decrease in inhibition of the catB endopeptidase activity. Compound **7**, on the other hand, proved to be a better exopeptidase activity inhibitor than its aminomethylated analogue (K_i = 426 ± 39 μM[30]) with constant of inhibition in the low micromolar range (K_i = 128 ± 21 μM, K_i' = 30 ± 10 μM, Table 1). The assay results for compounds **5**–**8** are indicating that the interaction of their mildly electrophilic amidoacetonitrile warhead with the catalytic cysteine did not take place, as the literature data show that the K_i values are substantially lower when the covalent interaction occurs.[23] The most promising compounds from this series proved to be compounds **9** and **10** with a larger side chain comprised of 1,3-substituted piperidine core at position 7 (Table 1). When using *Z*-Arg-Arg-AMC as a substrate, compounds **9** and **10** acted as uncompetitive inhibitors of catB, with K_i' of 8 ± 0 μM and 12 ± 1 μM, respectively. In addition, both compounds inhibited exopeptidase activity of catB with the same potency and in the same mode (**9**: K_i' = 13 ± 0 μM, **10**: K_i' = 18 ± 2 μM; Table 1). Interestingly, when we introduced the 2,3-dihydro-1*H*-indene (compound **11**) instead of the benzoxazole (**9**) or benzothiazole (**10**) on the piperidine nitrogen, no inhibition was observed. The same occurred when the methylene group was inserted between the piperidine and aromatic bicyclic system (compounds **12**–**14**, Table S1).

Small substituents at position 2 led to diminished inhibitory activity in comparison with nitroxoline, except for compounds **15** and **16** with Me and CN moiety, respectively, at position 2. These two compounds showed similar constants of inhibition for both catB activities as were determined for nitroxoline (Table S2 and Fig. S1). The nitrile-containing compounds **20**–**24** were poor inhibitors of both catB activities, with only compound **22** showing improved inhibition (endopeptidase activity: K_i' = 34 ± 1 μM; exopeptidase activity: K_i = 156 ± 48 μM, K_i' = 18 ± 5 μM, Table 1) in comparison with nitroxoline.

Unsurprisingly, the majority of compounds from the truncated series inhibited both catB activities poorly (Table S3), which indicates that both rings are needed for efficient binding into the active site of catB. Compounds **27** and **37** (Table S3) did, however, inhibit the exopeptidase activity with K_i values below 100 μM rendering these two molecules as interesting catB-inhibiting fragments.

In a previous study,[30] we showed that 4-methylpiperidine moiety attached at position 8 of the 5-nitroquinoline ring, results in increased exopeptidase activity inhibition in comparison with nitroxoline. Interestingly, the 8-substituted derivatives presented herein showed a particularly weak or even absence of inhibition of catB (Table S4). Only compounds **61** and **66** are of interest from this series, as they showed uncompetitive inhibition of both catB activities in the low micromolar range (Table 1). It is important to note here that the SARs of compounds **60**–**63** (Table S4) seem flat, because very small structural changes led to significant decrease in inhibitory activities.

Addition of an NO_2 group at position 7 of **15** (compound **S1**, Table S5) resulted in a loss of catB inhibitory activity, whereas there were no significant differences in inhibitory properties between compound **16** and its 5,7-dinitro analogue **S2** (Tables 1 and S5). The most potent dinitro nitroxoline derivative was compound **S5**, with a K_i' of 9 ± 1 μM for endopeptidase activity and K_i and K_i' of 154 ± 23 μM and 35 ± 12 μM, respectively, for exopeptidase activity (Table 1).

Recently, it was shown that the pH value of the assay buffer plays a more important role in the measurement of inhibitory activities in comparison with the choice of the substrate, i.e., the latter did not strongly affect the equilibrium between the endopeptidase (open) or exopeptidase (closed) form of catB.[22] To address the effect of pH on the inhibitory activity and to shift the equilibrium of catB to the closed conformation, we assayed the compounds from Table 1 using the 'small' endopeptidase substrate *Z*-Arg-Arg-AMC at pH 4.5 (Table S6). Given the fact that compounds presented in Table 1 are small in size (with exceptions of **9** and **10**), we were expecting improvements in inhibitory activities as a result of the proximity of histidines in the occluding loop (where the NO_2 group of inhibitors binds[28]) and other enzyme's binding subsites. In contrast to our expectations and for reasons currently unknown, all inhibitors exhibited higher K_i values under acidic assay conditions. The most striking difference was observed for compounds **9** and **10**, which showed a 30-fold reduction in K_i values (**9**: 8.2 μM at pH 6 versus 237 μM at pH 4.5; **10**: 12.0 μM at pH 6 versus 322 μM at pH 4.5; Table S6).

Our next step was to explore the effects of selected inhibitors (**6**–**10**, **15**, and **S5**) on the proteolysis of the ECM and tumor cell invasion *in vitro*. CatB is substantially involved in the progression of cancer, as it was shown that extracellular and intracellular catB activities contribute substantially to the turnover of ECM.[8,11,35] To investigate the impact of inhibitors on ECM degradation, we evaluated their effects on the degradation of DQ-collagen IV by MCF-10A neoT cells. Collagen type IV is a major constituent of the ECM that can be fluorescently tagged and gives after enzymatic cleavage bright green fluorescence. Moreover, we have shown previously that MCF-10A neoT cells degrade DQ-collagen IV inside cells and extracellularly.[29] To quantify the extracellular and intracellular degradation of the DQ-collagen IV, spectrofluorimetry and flow cytometry were employed (Fig. 3). Compounds **6** (5 μM), **9** (1.25 μM), and **10** (1.25 μM) showed the most potent reduction of the

Table 1
Cathepsin B inhibitory activities of selected nitroxoline derivatives.

		Z-Arg-Arg-AMC		Abz-Gly-Ile-Val-Arg-Ala-Lys(Dnp)—OH	
		K_i (μM)[a]	K_i' (μM)[a]	K_i (μM)[a]	K_i' (μM)[a]
7-Carboxamido substituted derivatives					
6	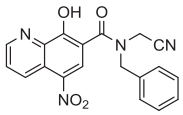	182 ± 31[b]	64 ± 13[b]	185 ± 5[b]	32 ± 7[b]
7	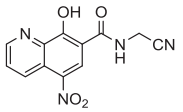	–	67 ± 10[c]	128 ± 21[b]	30 ± 10[b]
8	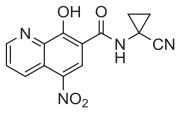	–	124 ± 14[c]	185 ± 2[d]	
9	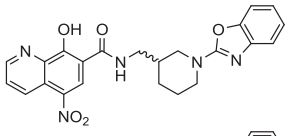	–	8 ± 0[c]	–	13 ± 0[c]
10	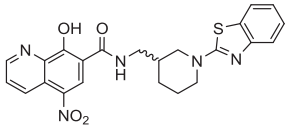	–	12 ± 1[c]	–	18 ± 2[c]
2-Substituted derivatives					
15	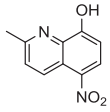	181 ± 14[b]	99 ± 18[b]	469 ± 58[b]	77 ± 20[b]
16	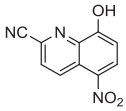	142 ± 5[b]	68 ± 0[b]	214 ± 30[d]	
22	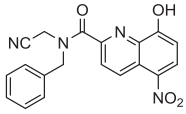	–	34 ± 1[c]	156 ± 48[b]	18 ± 5[b]
8-Substituted derivatives					
44	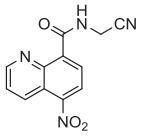	240 ± 35[e]	–	190 ± 3[d]	
49[f]	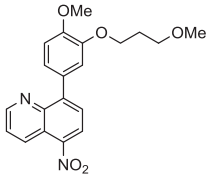	323 ± 3[d]		118 ± 0[b]	22 ± 0[b]
61[f]	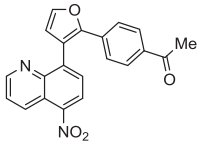	–	46 ± 16[c]	–	11 ± 1[c]

(*continued on next page*)

Table 1 (*continued*)

		Z-Arg-Arg-AMC		Abz-Gly-Ile-Val-Arg-Ala-Lys(Dnp)—OH	
		K_i (μM)[a]	K_i' (μM)[a]	K_i (μM)[a]	K_i' (μM)[a]
66[f]	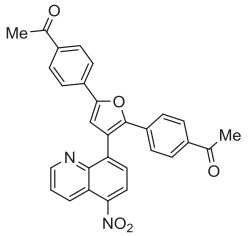	–	39 ± 3[c]	–	13 ± 8[c]
2-Substituted-5,7-dinitro derivatives					
S5	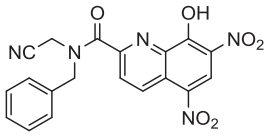	–	9 ± 1[c]	154 ± 23[b]	35 ± 12[b]
S6	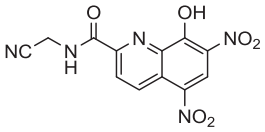	160 ± 42[d]		201 ± 89[b]	34 ± 8[b]

[a] K_i and K_i' values are the mean ± SD (n = 3).
[b] Mixed inhibition.
[c] Uncompetitive inhibition.
[d] Noncompetitive inhibition.
[e] Competitive inhibition.
[f] Poorly soluble compounds.

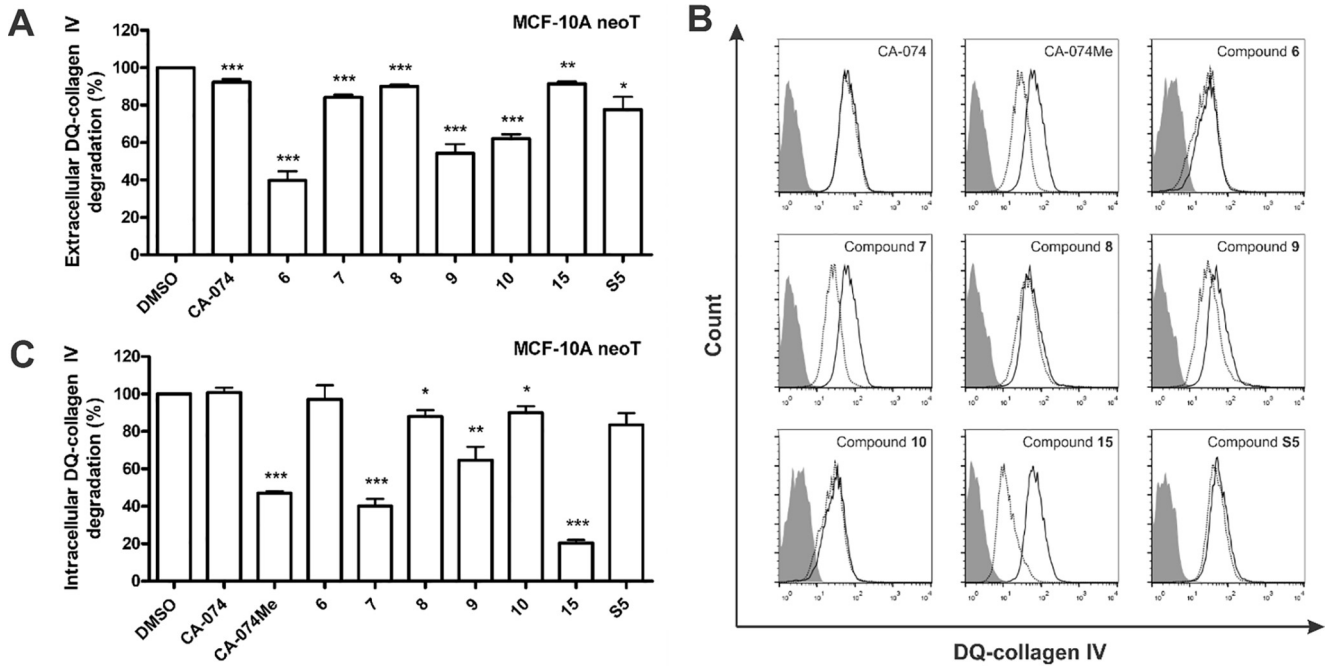

Fig. 3. Nitroxoline derivatives inhibit extracellular and intracellular DQ-collagen IV degradation. (A) Extracellular degradation of DQ-collagen IV by MCF-10A neoT cells (5×10^4) in the presence of DMSO or respective compound (5 μM for compounds **6**, **7**, **8**, **S5**, and CA-074, 2.5 μM for compounds **15**, or 1.25 μM for compounds **9** and **10**) was analyzed by monitoring the fluorescence intensity of extracellular degradation product using spectrofluorimetry. Data are presented as the mean ± SEM (n = 3) and experiments were performed in six replicates. (B) Intracellular DQ-collagen IV degradation by MCF-10A neoT cells (6×10^4) after treatment with DMSO (solid black line) or respective compound (50 μM for compounds **6**, **7**, **8**, **S5**, CA-074, and CA-074Me, 25 μM for compound **15**, or 12.5 μM for compounds **9** and **10**, dotted black line) was monitored using flow cytometry. Gray histograms denote unlabeled cells. (C) Reduction of intracellular DQ-collagen IV in the presence of DMSO or suitable compound (50 μM for compounds **6**, **7**, **8**, **S5**, CA-074, and CA-074Me, 25 μM for compound **15**, or 12.5 μM for compounds **9** and **10**) as assayed by flow cytometry. Data are presented as the mean ± SEM (n = 3) and the experiments were performed in duplicates. $^{*}P < 0.05$, $^{**}P < 0.01$, $^{***}P < 0.001$.

Please cite this article in press as: Sosič I., et al. Bioorg. Med. Chem. Lett. (2018), https://doi.org/10.1016/j.bmcl.2018.02.042

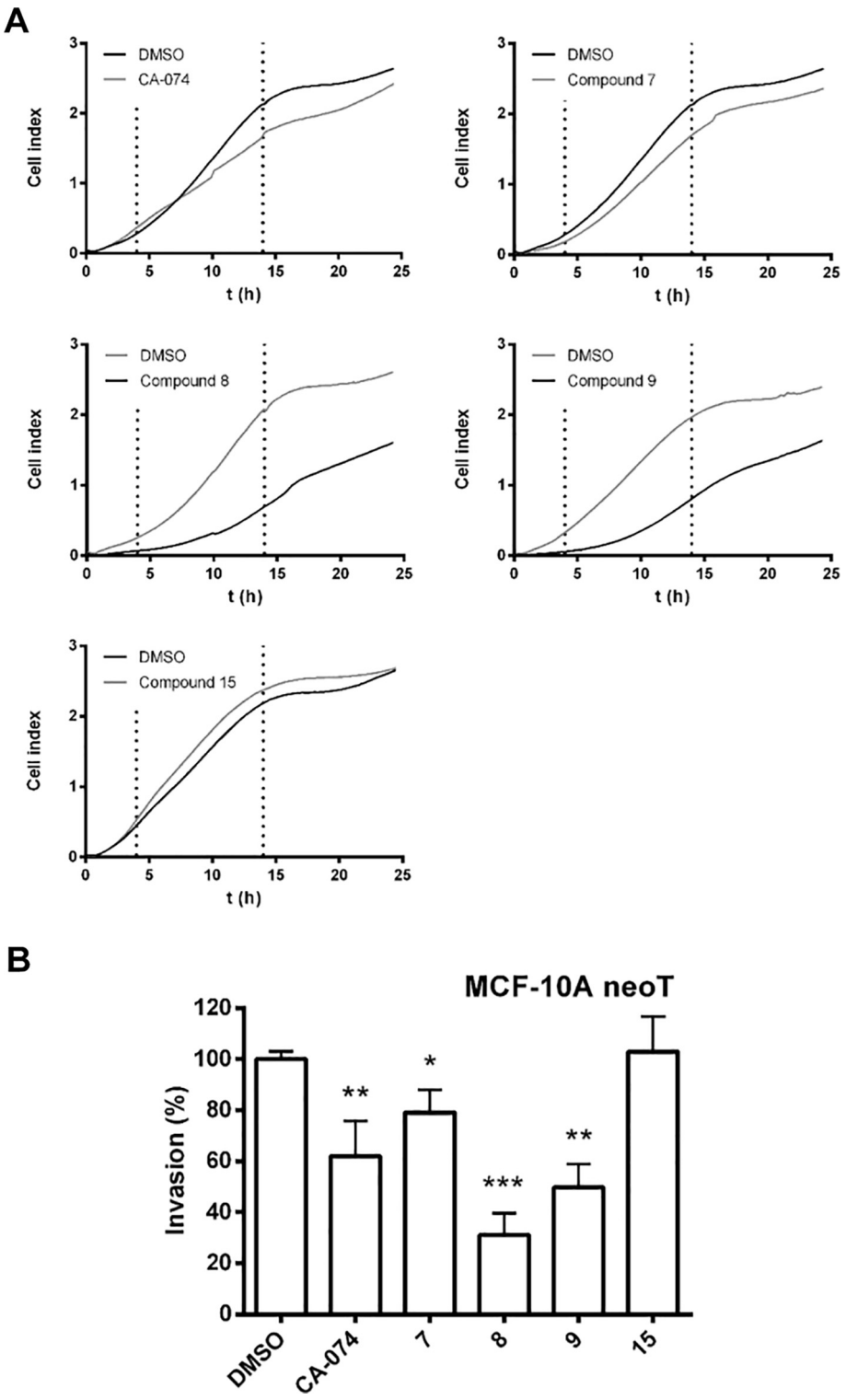

Fig. 4. Impact of compounds **7**–**9** and **15** on invasion of MCF-10A neoT cells monitored in real-time. (A) MCF-10A neoT cells (3×10^4) were seeded on top of Matrigel (1 mg/mL) coated upper compartments of CIM-plate 16. DMSO (0.05%) or respective compound (5 μM for compounds **7**, **8**, and CA-074, 2.5 μM for compounds **15**, or 1.25 μM for compound **9**) was added to the growth medium in the upper and lower compartments of the CIM-plate 16. Cell invasion was monitored continuously for 72 h by measuring impedance data (reported as CI) using the xCELLigence system. (B) The slopes (1/h) in the time interval between 4 and 14 h correlated with the ability of the cells to invade and were used to calculate the percentage of invasion (%), presented as means ± SEM (n = 2). The experiments were performed in triplicates. $^{*}P < 0.05$, $^{**}P < 0.01$, $^{***}P < 0.001$.

extracellular DQ-collagen IV degradation by ~ 60%, ~45%, and ~ 40%, respectively, whereas other compounds (**7**, **8**, **15** and **S5**) showed less pronounced effects (Fig. 3A). The results from intracellular degradation assay showed that compounds **7** (50 μM), **8** (50 μM), **9** (12.5 μM), and **15** (25 μM) proved to be the most promising, as they inhibited intracellular DQ-collagen IV degradation by ~60%, ~15%, ~35%, and ~80%, respectively (Figs. 3B and 3C). Compounds **6** (50 μM), **10** (12.5 μM), and **S5** (50 μM) inhibited this process by less than 10% (**6** and **10**) or showed statistically non-significant results (**S5**) (Figs. 3B and 3C). Similarly as determined previously,[36]

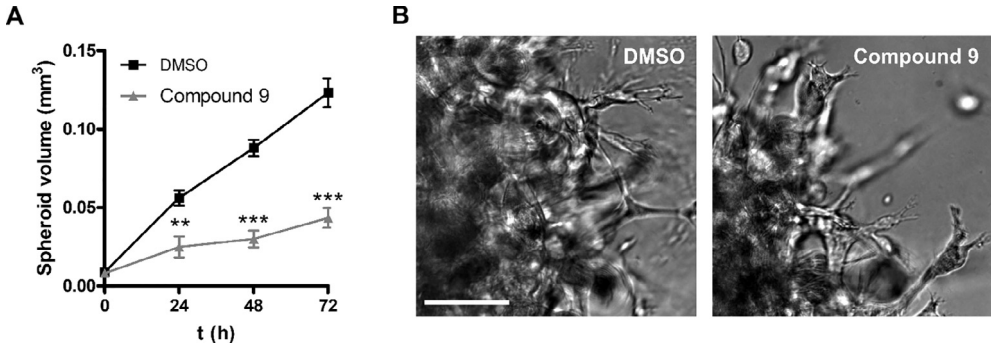

Fig. 5. Compound **9** impairs invasion of U-87 MG cells in a three-dimensional *in vitro* model of tumor invasion. (A) U-87 MG spheroids were implanted in Matrigel (5 mg/mL) and covered with growth medium, both containing inhibitor **9** (1.25 μM) or DMSO (0.05%) as a control. The spheroid dimensions were measured for up to three days and the spheroid volume was calculated. Data are presented as means ± SEM (n = 2). (B) Representative images of U-87 MG spheroids obtained at day three after implantation. Scale bar, 100 μm. $^{**}P < 0.01$, $^{***}P < 0.001$.

only the cell-permeable ester analogue of the positive control, CA-074Me (50 μM), impaired intracellular degradation of the ECM by ~55%, whereas CA-074 (50 μM) failed to show activity inside cells.

The inhibition of both extracellular and intracellular catB is needed for significant attenuation of tumor cell invasion.[37] Therefore, compounds **7**–**9** and **15** that showed cell-permeable characteristics were selected to assess their impact on tumor-cell invasion. As a first method, the invasion of tumor cells through Matrigel, as a model of the ECM, was monitored in real time using the xCELLigence system.[38] This two-chamber-based system measures electrical impedance, expressed as cell index, across microelectrodes integrated in the membrane separating the top and bottom compartments of tissue culture CIM-plates (Fig. 4A). In this assay, compound **8** (5 μM) significantly abrogated the invasion of MCF-10A neoT cells by ~70% compared to the DMSO control (Fig. 4B), followed by compound **9** (1.25 μM), which showed ~50% inhibition of the invasion. Interestingly, compound **15** was not active despite showing potent inhibition of intracellular degradation of DQ-collagen IV. Compound **7**, on the other hand, which was also effective intracellularly, reduced invasion by ~20% (Fig. 4B); probably as a result of better inhibition of the extracellular ECM degradation in comparison with **15**. For comparison, an irreversible catB-specific inhibitor CA-074, which was used as a control compound, inhibited cell invasion by ~40%.

To further corroborate the results from two-dimensional assay, compound **9** was analyzed by an *in vitro* three-dimensional invasion assay. Multicellular tumor spheroids (MCTS) from U-87 MG cells were prepared according to the hanging drop method[39] and implanted in ECM-mimicking matrix (Matrigel). For U-87 MG cells, we have previously shown that they express high levels of catB, efficiently form MCTS, and invade Matrigel.[29] MCTS more closely represent a tumor *in vivo* by mimicking the early, avascular stages of tumor growth and are therefore, more representative as a model of tumor cell invasion compared to those involving cell monolayers.[39] During the three day experiment, the U-87 MG MCTS showed steady growth (Fig. 5A) and formed radially invasive strands around the spheroid (Fig. 5B). Addition of compound **9** (1.25 μM) significantly impaired tumor growth in a three-dimensional experimental setting (Fig. 5A) confirming its encouraging anti-tumor characteristics.

For compounds **7**–**9** and **15** that were assayed in models of tumor invasion, selectivity against cathepsin H (catH) and cathepsin L (catL) was evaluated (Table S7). These results showed that compound **9** had the same affinity for catL (K_i = 5 ± 0 μM, Table S7) as for catB (endopeptidase activity: K_i' = 8 ± 0 μM; exopeptidase activity: K_i' = 13 ± 0 μM, Table 1), whereas lower preference was shown for catH (K_i = 108 ± 26 μM, Table S7). This fact along with evidence that catL is involved in proteolytic events during tumor progression[16,27] could, in part, explain very potent effects of compound **9** in both cell-based tumor models at concentrations that are lower than its constants of inhibition on isolated enzymes. In addition, we cannot exclude possible effects on other targets, such as type 2 methionine aminopeptidase and sirtuin, which were identified to be targets for nitroxoline.[40] Similarly, compounds **7** and **8** also showed a preference for catB inhibition over catH, but not over catL (Table S7), whereas compound **15** was non-selective, as it inhibited all three enzymes in a similar concentration range, i.e., from approximately 80 to 120 μM.

To exclude the possibility that the inhibition of ECM degradation and tumor cell invasion resulted from the compound-induced cell-toxicity, all effects of compounds in functional assays (**6**–**10**, **15**, and **S5**) were studied at concentrations, which did not cause a decrease in cell viability. These concentrations were selected by performing cell viability studies that are presented in the Supplementary data (Fig. S3).

In summary, we prepared a set of more than 60 nitroxoline-based derivatives to complement previous results and to further explore their SARs as a catB-inhibiting core. Despite the fact that significant improvement in *in vitro* catB inhibition was not achieved in comparison with previous results[30] several derivatives showed promising efficacy in tumor-cell-based assays, where they inhibited extracellular and intracellular degradation of ECM and tumor-cell invasion. Moreover, the fragment-like characteristics of the majority of compounds represent solid foundation for further ligand- and structure-based optimization of nitroxoline derivatives as catB inhibitors (see also ligand efficiency changes in comparison with previous compounds, Table S8). To achieve a significant leap in the inhibitory activity, additional optimizations of the substituents at positions 2 and 7 are needed, followed by proper positioning of the mildly electrophilic functional group to form reversible covalent interaction with the catalytic cysteine. Furthermore, incorporation of other cysteine-selective electrophilic warheads is possible and will represent a subject of our following endeavors in the field of nitroxoline-based catB inhibitors.

Acknowledgments

The authors thank all undergraduate students that helped with the syntheses of compounds.

Funding sources

This work was supported by the Slovenian Research Agency: research core funding No. P1-0208, grant number J4-5529 (D) to J.K., and grant number Z1-7181 (B) to I.S.: Optimization of

nitroxoline-based inhibitors of cathepsin B as potential drugs for the treatment of cancer.

A. Supplementary data

Supplementary data (tables with inhibition data for all compounds, assays results on cathepsins H and L, catB inhibitory activities of selected nitroxoline derivatives at pH 4.5 with *Z*-Arg-Arg-AMC as a substrate, supporting schemes and figures, full experimental section, synthetic procedures, and elemental analyses data for final compounds) associated with this article can be found, in the online version, at https://doi.org/10.1016/j.bmcl.2018.02.042.

References

1. Fonović M, Turk B. Cysteine cathepsins and extracellular matrix degradation. *Biochim Biophys Acta, Gen Subj*. 2014;1840:2560–2570.
2. Turk V, Stoka V, Vasiljeva O, et al. Cysteine cathepsins: from structure, function and regulation to new frontiers. *Biochim Biophys Acta*. 2012;1824:68–88.
3. Illy C, Quraishi O, Wang J, Purisima E, Vernet T, Mort JS. Role of the occluding loop in cathepsin B activity. *J Biol Chem*. 1997;272:1197–1202.
4. Musil D, Zucic D, Turk D, et al. The refined 2.15 Å X-ray crystal structure of human liver cathepsin B: the structural basis for its specificity. *EMBO J*. 1991;10:2321–2330.
5. Krupa JC, Hasnain S, Nägler DK, Ménard R, Mort JS. S2′ substrate specificity and the role of His110 and His111 in the exopeptidase activity of human cathepsin B. *Biochem. J.*. 2002;361:613–619.
6. Nägler DK, Storer AC, Portaro FCV, Carmona E, Juliano L, Ménard R. Major increase in endopeptidase activity of human cathepsin B upon removal of occluding loop contacts. *Biochemistry*. 1997;36:12608–12615.
7. Almeida PC, Nantes IL, Chagas JR, et al. Cathepsin B activity regulation. heparin-like glycosaminogylcans protect human cathepsin B from alkaline pH-induced inactivation. *J Biol Chem*. 2001;276:944–951.
8. Roshy S, Sloane BF, Moin K. Pericellular cathepsin B and malignant progression. *Cancer Metastasis Rev*. 2003;22:271–286.
9. Skrzydlewska E, Sulkowska M, Koda M, Sulkowski S. Proteolytic-antiproteolytic balance and its regulation in carcinogenesis. *World J Gastroenterol*. 2005;11:1251–1266.
10. Koblinski JE, Ahram M, Sloane BF. Unraveling the role of proteases in cancer. *Clin Chim Acta*. 2000;291:113–135.
11. Premzl A, Zavašnik-Bergant V, Turk V, Kos J. Intracellular and extracellular cathepsin B facilitate invasion of MCF-10A NeoT cells through reconstituted extracellular matrix. *In Vitro Exp Cell Res*. 2003;283:206–214.
12. Kostoulas G, Lang A, Nagase H, Baici A. Stimulation of angiogenesis through cathepsin B inactivation of the tissue inhibitors of matrix metalloproteinases. *FEBS Lett*. 1999;455:286–290.
13. Premzl A, Turk V, Kos J. Intracellular proteolytic activity of cathepsin B is associated with capillary-like tube formation by endothelial cells in vitro. *J Cell Biochem*. 2006;97:1230–1240.
14. Cavallo-Medved D, Rudy D, Blum G, Bogyo M, Caglic D, Sloane BF. Live-cell imaging demonstrates extracellular matrix degradation in association with active cathepsin B in caveolae of endothelial cells during tube formation. *Exp Cell Res*. 2009;315:1234–1246.
15. Burchard M, Mignot G, Derangère V, et al. Chemotherapy-triggered cathepsin B release in myeloid-derived suppressor cells activates the nlrp3 inflammasome and promotes tumor growth. *Nat Med*. 2013;19:57–64.
16. Gocheva V, Zeng W, Ke D, et al. Distinct roles for cysteine cathepsin genes in multistage tumorigenesis. *Genes Dev*. 2006;20:543–556.
17. Vasiljeva O, Papazoglou A, Krüger A, et al. Tumor cell-derived and macrophage-derived cathepsin B promotes progression and lung metastasis of mammary cancer. *Cancer Res*. 2006;66:5242–5250.
18. Sevenich L, Schurigt U, Sachse K, et al. Synergistic antitumor effects of combined cathepsin B and cathepsin Z deficiencies on breast cancer progression and metastasis in mice. *Proc Natl Acad Sci USA*. 2010;107:2497–2502.
19. Vasiljeva O, Korovin M, Gajda M, et al. Reduced tumour cell proliferation and delayed development of high-grade mammary carcinomas in cathepsin B-deficient mice. *Oncogene*. 2008;27:4191–4199.
20. Gopinathan A, Denicola GM, Frese KK, et al. Cathepsin B promotes the progression of pancreatic ductal adenocarcinoma in mice. *Gut*. 2012;61:877–884.
21. Kos J, Mitrović A, Mirković B. The current stage of cathepsin B inhibitors as potential anticancer agents. *Future Med Chem*. 2014;6:1355–1371.
22. Schmitz J, Li T, Bartz U, Gütschow M. Cathepsin B inhibitors: combining dipeptide nitriles with an occluding loop recognition element by click chemistry. *ACS Med Chem Lett*. 2016;7:211–216.
23. Frizler M, Stirnberg M, Sisay MT, Gütschow M. Development of nitrile-based peptidic inhibitors of cysteine cathepsins. *Curr Top Med Chem*. 2010;10:294–322.
24. Frizler M, Lohr F, Lülsdorff M, Gütschow M. Facing the *gem*-dialkyl effect in enzyme inhibitor design: preparation of homocycloleucine-based azadipeptide nitriles. *Chem Eur J*. 2011;17:11419–11423.
25. Turk B. Targeting proteases: successes, failures and future prospects. *Nat Rev Drug Discov*. 2006;5:785–799.
26. Kramer L, Turk D, Turk B. The future of cysteine cathepsins in disease management. *Trends Pharmacol Sci*. 2017;38:873–898.
27. Olson OC, Joyce JA. Cysteine cathepsin proteases: regulators of cancer progression and therapeutic response. *Nat Rev Cancer*. 2015;15:712–729.
28. Mirković B, Renko M, Turk S, et al. Novel mechanism of cathepsin B inhibition by antibiotic nitroxoline and related compounds. *ChemMedChem*. 2011;6:1351–1356.
29. Mirković B, Markelc B, Butinar M, et al. Nitroxoline impairs tumor progression *in vitro* and *in vivo* by regulating cathepsin B activity. *Oncotarget*. 2015;6:19027–19042.
30. Sosič I, Mirković B, Arenz K, Štefane B, Kos J, Gobec S. Development of new cathepsin B inhibitors: combining bioisosteric replacements and structure-based design to explore the structure-activity relationships of nitroxoline derivatives. *J Med Chem*. 2013;56:521–533.
31. Mitrović A, Sosič I, Kos Š, et al. Addition of 2-(ethylamino)acetonitrile group to nitroxoline results in significantly improved anti-tumor activity in vitro and in vivo. *Oncotarget*. 2017;8:59136–59147.
32. Ogrizek M, Turk S, Lešnik S, et al. Molecular dynamics to enhance structure-based virtual screening on cathepsin B. *J Comput Aided Mol Des*. 2015;29:707–712.
33. Knez D, Brus B, Coquelle N, et al. Structure-based development of nitroxoline derivatives as potential multifunctional anti-Alzheimer agents. *Bioorg Med Chem*. 2015;23:4442–4452.
34. Brodnik H, Požgan F, Štefane B. Synthesis of 8-heteroaryl nitroxoline analogues *via* one-pot sequential Pd-catalyzed coupling reactions. *Org Biomol Chem*. 2016;14:1969–1981.
35. Mohamed MM, Sloane BF. Cysteine cathepsins: multifunctional enzymes in cancer. *Nat Rev Cancer*. 2006;6:764–775.
36. Mitrović A, Mirković B, Sosič I, Gobec S, Kos J. Inhibition of endopeptidase and exopeptidase activity of cathepsin B impairs extracellular matrix degradation and tumour invasion. *Biol Chem*. 2016;397:165–174.
37. Szpaderska AM, Frankfater A. An intracellular form of cathepsin B contributes to invasiveness in cancer. *Cancer Res*. 2001;61:3493–3500.
38. Eisenberg MC, Kim Y, Li R, Ackerman WE, Kniss DA, Friedman A. Mechanistic modeling of the effects of myoferlin on tumor cell invasion. *Proc Natl Acad Sci USA*. 2011;108:20078–20083.
39. Kelm JM, Timmins NE, Brown CJ, Fussenegger M, Nielsen LK. Method for generation of homogeneous multicellular tumor spheroids applicable to a wide variety of cell types. *Biotechnol Bioeng*. 2003;83:173–180.
40. Shim JS, Matsui Y, Bhat S, et al. Effect of nitroxoline on angiogenesis and growth of human bladder cancer. *J Natl Cancer Inst*. 2010;102:1855–1873.